Electronic Supplementary Material (ESI) for Physical Chemistry Chemical Physics


# Supporting Information

## Photoelectron spectroscopy of lithium and gold alloyed boron oxide clusters: charge transfer complexes, covalent gold, hyperhalogen, and dual three-center four-electron hyperbonds

Wen-Juan Tian,[a] Hong-Guang Xu,[b] Xiang-Yu Kong,[b,c] Qiang Chen,[a] Wei-Jun Zheng,[b,c,*] Hua-Jin Zhai,[a,*] and Si-Dian Li[a,*]

[a]*Nanocluster Laboratory, Institute of Molecular Science, Shanxi University, Taiyuan 030006, China*

[b]*State Key Laboratory of Molecular Reaction Dynamics, Institute of Chemistry, Chinese Academy of Sciences, Beijing 100190, China*

[c]*University of Chinese Academy of Sciences, Beijing 100049, China*

E-mail: zhengwj@iccas.ac.cn (W.J.Z.); hj.zhai@sxu.edu.cn (H.J.Z.); lisidian@sxu.edu.cn (S.D.L.)

**Complete citation of ref 30**

**Table S1.** Calculated one-electron detachment energies (ADEs and VDEs) of the second lowest-lying isomers of $C_s$ $B_2O_3^-$, $C_{\infty v}$ $LiB_2O_3^-$, and $C_{\infty v}$ $AuB_2O_3^-$ anions at DFT and the Outer Valence Green's Function (OVGF) levels, as compared to the corresponding experimental values.

**Tables S2-S5.** NRT analyses of optimized ground-state structures of $B_2O_3^-$, $LiB_2O_3^-$, $AuB_2O_3^-$ and $LiAuB_2O_3^-$.

**Figure S1.** Photoelectron spectrum of $B_2O_3^-$ cluster recorded with 266 nm photons.

**Figures S2-S5.** Optimized geometries of top ten low-lying isomers of $B_2O_3^-$, $LiB_2O_3^-$, $AuB_2O_3^-$ and $LiAuB_2O_3^-$, along with their relative energies in kcal/mol at MPW1PW91. Also shown are the relative energies at the {CCSD(T)//MPW1PW91} level for top five low-lying isomers.

**Figures S6-S9.** Pictures of molecular orbitals for ground-state structures of $B_2O_3^-$, $LiB_2O_3^-$, $AuB_2O_3^-$, and $LiAuB_2O_3^-$.

**Figure S10.** Natural charge distribution of optimized ground-state structures of $B_2O_3^-$, $LiB_2O_3^-$, $AuB_2O_3^-$, and $LiAuB_2O_3^-$ (a–d) and their neutral structures (e-h).

**Complete citation of ref 30**

30 M. J. Frisch, G. W. Trucks, H. B. Schlegel, G. E. Scuseria, M. A. Robb, J. R. Cheeseman, G. Scalmani, V. Barone, B. Mennucci, G. A. Petersson, H. Nakatsuji, M. Caricato, X. Li, H. P. Hratchian, A. F. Izmaylov, J. Bloino, G. Zheng, J. L. Sonnenberg, M. Hada, M. Ehara, K. Toyota, R. Fukuda, J. Hasegawa, M. Ishida, T. Nakajima, Y. Honda, O. Kitao, H. Nakai, T. Vreven, J. A. Montgomery, Jr., J. E. Peralta, F. Ogliaro, M. Bearpark, J. J. Heyd, E. Brothers, K. N. Kudin, V. N. Staroverov, R. Kobayashi, J. Normand, K. Raghavachari, A. Rendell, J. C. Burant, S. S. Iyengar, J. Tomasi, M. Cossi, N. Rega, J. M. Millam, M. Klene, J. E. Knox, J. B. Cross, V. Bakken, C. Adamo, J. Jaramillo, R. Gomperts, R. E. Stratmann, O. Yazyev, A. J. Austin, R. Cammi, C. Pomelli, J. W. Ochterski, R. L. Martin, K. Morokuma, V. G. Zakrzewski, G. A. Voth, P. Salvador, J. J. Dannenberg, S. Dapprich, A. D. Daniels, Ö. Farkas, J. B. Foresman, J. V. Ortiz, J. Cioslowski and D. J. Fox, Gaussian, Inc., Wallingford CT, 2009.

***Table S1.*** Calculated one-electron detachment energies (ADEs and VDEs) of the second lowest-lying isomers of $C_s$ $B_2O_3^-$, $C_{\infty v}$ $LiB_2O_3^-$, and $C_{\infty v}$ $AuB_2O_3^-$ anions at DFT and the Outer Valence Green's Function (OVGF) levels, as compared to the corresponding experimental values.[a]

| | | | Experimental[b] | | Theoretical | | |
|---|---|---|---|---|---|---|---|
| Species | Feature | Final state | ADE[c] | VDE | ADE[d] | VDE[d] | OVGF[e] |
| $B_2O_3^-$ | X | $^1A'$ | 1.45[f] | 2.22 | 0.66 (0.39) | 2.18 (1.73) | 1.92 |
| | A | $^3A''$ | | ~5.9 | | 5.81 (5.81) | 6.21 |
| $LiB_2O_3^-$ | X | $^2\Sigma^+$ | 4.25 | 4.43 | -[g] | 5.57 (5.37) | 5.53 |
| $AuB_2O_3^-$ | X | $^2\Sigma^+$ | 6.05 | 6.17 | 6.00 (6.12) | 6.38 (6.13) | 6.53 |

[a] All energies are in eV.

[b] Estimated experimental uncertainties: ±0.08 eV.

[c] Electron affinity of the neutral cluster.

[d] ADEs and VDEs calculated at the MPW1PW91/Au/Stuttgart/B,O,Li/6-311+G(d,p) level. CCSD(T) values are indicated in the parentheses.

[e] Calculated at the OVGF/Au/Stuttgart/B,O,Li/6-311+G(d,p) level.

[f] Due to the large anion-to-neutral geometric changes, the 0-0 transition may be negligibly small. The observed ADE should be considered as an upper limit of the true electron affinity.

[g] The ADE of $C_{\infty v}$ $LiB_2O_3^-$ ($[O{\equiv}B{-}Li{-}O{\equiv}B{\equiv}O]^-$) is missing due to the fact that its neutral dissociates during structural optimization.

***Table S2.*** Natural resonance theory (NRT) bond orders and atomic valencies of $C_{2v}$ $B_2O_3^-$ ($^2A_1$).

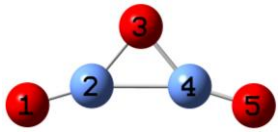


$C_{2v}$ $B_2O_3^-$ ($^2A_1$)

| | | Natural Bond Order | | | Natural Atomic Valency | | |
|---|---|---|---|---|---|---|---|
| | | $O_1$-$B_2$ | $B_2$-$O_3$ | $B_2$-$B_4$ | $O_1$ | $B_2$ | $O_3$ |
| NRT | t | 2.90 | 1.02 | 0.47 | 2.90 | 4.39 | 2.03 |
| | c | 0.90 | 0.37 | 0.43 | 0.90 | 1.70 | 0.74 |
| | i | 2.00 | 0.65 | 0.04 | 2.00 | 2.69 | 1.29 |

***Table S3.*** Natural resonance theory (NRT) bond orders and atomic valencies of $C_{\infty v}$ $LiB_2O_3^-$ ($^1\Sigma^+$).


$C_{\infty v}$ $LiB_2O_3^-$ ($^1\Sigma$)

| | | Natural Bond Order | | | | | Natural Atomic Valency | | | | | |
|---|---|---|---|---|---|---|---|---|---|---|---|---|
| | | $B_1$-$O_2$ | $O_2$-$Li_3$ | $Li_3$-$O_4$ | $O_4$-$B_5$ | $B_5$-$O_6$ | $B_1$ | $O_2$ | $Li_3$ | $O_4$ | $B_5$ | $O_6$ |
| NRT[a] | t | 3.00 | 0.01 | 0.01 | 1.80 | 2.19 | 3.00 | 3.01 | 0.02 | 1.81 | 4.00 | 2.19 |
| | c | 0.76 | 0.00 | 0.00 | 0.59 | 0.80 | 0.76 | 0.76 | 0.00 | 0.59 | 1.40 | 0.80 |
| | i | 2.24 | 0.01 | 0.01 | 1.21 | 1.39 | 2.24 | 2.25 | 0.02 | 1.22 | 2.60 | 1.39 |

[a] $C_{\infty v}$ $LiB_2O_3^-$ ($^1\Sigma$) possesses three resonance structures:

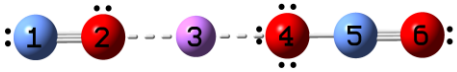


$NRT_1$ (46%)


$NRT_2$ (28%)


$NRT_3$ (24%)

***Table S4.*** Natural resonance theory (NRT) bond orders and atomic valencies of $C_s$ $AuB_2O_3^-$ ($^1A'$).

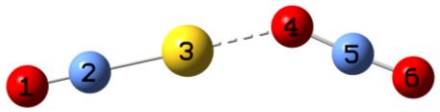


$C_s$ $AuB_2O_3^-$ ($^1A'$)

| | | Natural Bond Order | | | | | Natural Atomic Valency | | | | | |
|---|---|---|---|---|---|---|---|---|---|---|---|---|
| | | $O_1$-$B_2$ | $B_2$-$Au_3$ | $Au_3$-$O_4$ | $O_4$-$B_5$ | $B_5$-$O_6$ | $O_1$ | $B_2$ | $Au_3$ | $O_4$ | $B_5$ | $O_6$ |
| NRT[a] | t | 2.95 | 1.00 | 0.06 | 1.75 | 2.22 | 2.95 | 3.97 | 1.06 | 1.82 | 3.99 | 2.22 |
| | c | 1.07 | 0.79 | 0.00 | 0.56 | 0.81 | 1.07 | 1.86 | 0.79 | 0.56 | 1.38 | 0.81 |
| | i | 1.88 | 0.21 | 0.06 | 1.19 | 1.41 | 1.88 | 2.11 | 0.27 | 1.26 | 2.61 | 1.41 |

[a] $C_s$ $AuB_2O_3^-$ ($^1A'$) possesses three resonance structures:

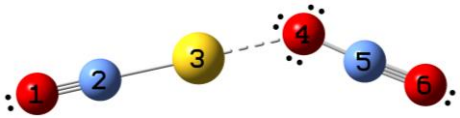


$NRT_1$ (41%)

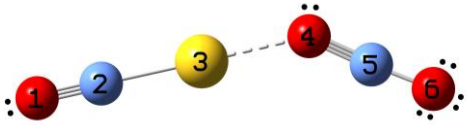


$NRT_2$ (21%)

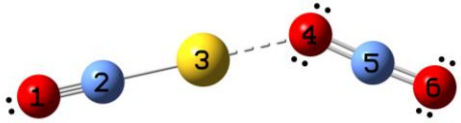


$NRT_3$ (21%)

***Table S5***. Natural resonance theory (NRT) bond orders and atomic valencies of $C_{\infty v}$ $LiAuB_2O_3^-$ ($^2\Sigma^+$).

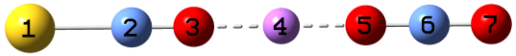


$C_{\infty v}$ $LiAuB_2O_3^-$ ($^2\Sigma$)

| | | Natural Bond Order | | | | | | Natural Atomic Valency | | | | | | |
|---|---|---|---|---|---|---|---|---|---|---|---|---|---|---|
| | | $Au_1$-$B_2$ | $B_2$-$O_3$ | $O_3$-$Li_4$ | $Li_4$-$O_5$ | $O_5$-$B_6$ | $B_6$-$O_7$ | $Au_1$ | $B_2$ | $O_3$ | $Li_4$ | $O_5$ | $B_6$ | $O_7$ |
| NRT[a] | t | 1.05 | 2.94 | 0.01 | 0.01 | 1.78 | 2.21 | 1.05 | 3.99 | 2.95 | 0.01 | 1.79 | 4.00 | 2.21 |
| | c | 0.57 | 0.87 | 0.00 | 0.00 | 0.58 | 0.81 | 0.57 | 1.45 | 0.87 | 0.00 | 0.58 | 1.40 | 0.81 |
| | i | 0.48 | 2.07 | 0.01 | 0.01 | 1.20 | 1.40 | 0.48 | 2.54 | 2.08 | 0.01 | 1.21 | 2.60 | 1.40 |

[a] $C_{\infty v}$ $LiAuB_2O_3^-$ ($^2\Sigma$) possesses three resonance structures:

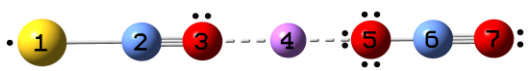


$NRT_1$ (44%)

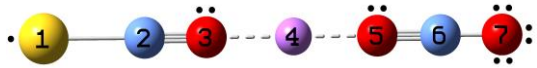


$NRT_2$ (24%)

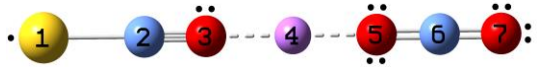


$NRT_3$ (23%)

***Figure S1.*** Photoelectron spectrum of $B_2O_3^-$ cluster recorded with 266 nm photons.

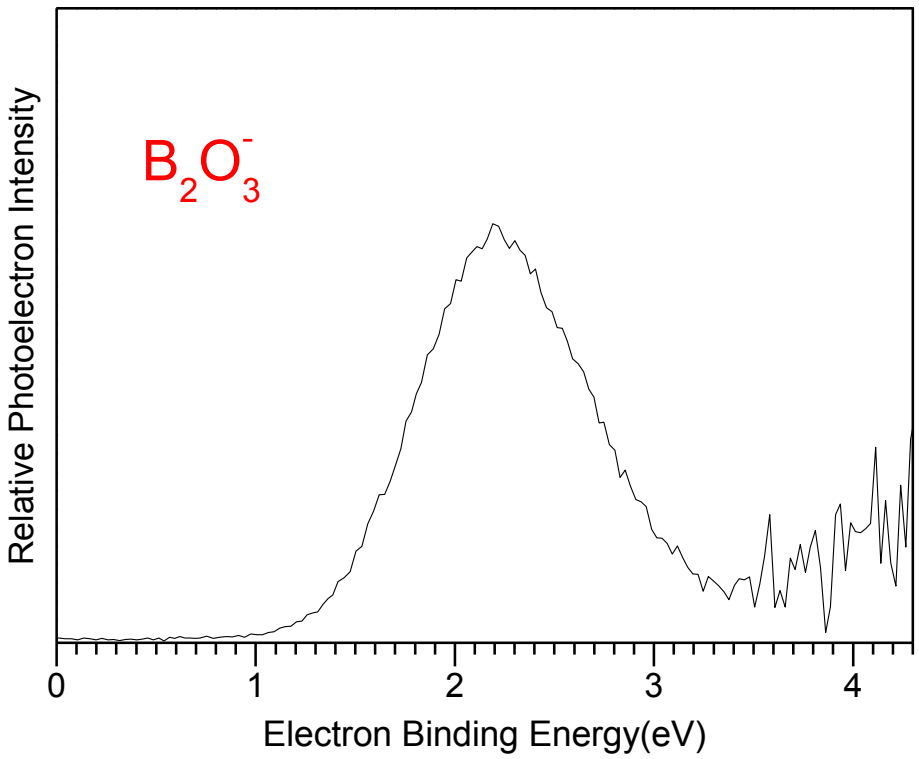

***Fig S2.*** Optimized geometries of top ten low-lying isomers of $B_2O_3^-$ along with their relative energies in kcal/mol at MPW1PW91. Also shown are the relative energies at the {CCSD(T)//MPW1PW91} level for top five low-lying isomers.

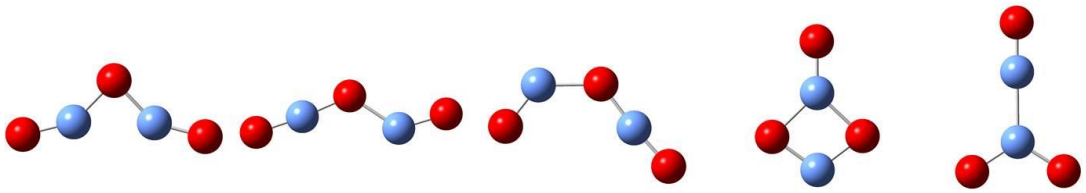

$C_{2v}$ ($^2A_1$) 0.00 {0.00} | $C_s$ ($^2A'$) +2.81 {+0.28} | $C_s$ ($^2A'$) +4.46 {+2.48} | $C_{2v}$ ($^2A_1$) +4.92 {+5.18} | $C_{2v}$ ($^2B_2$) +33.22 {+32.12}

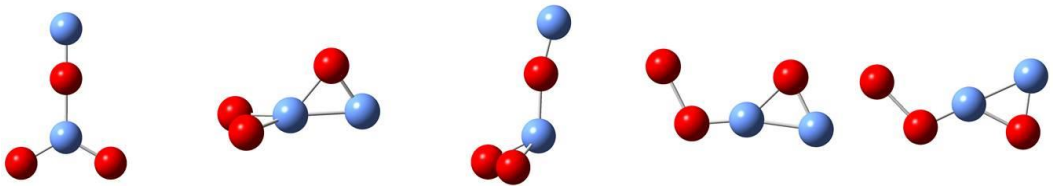

$C_{2v}$ ($^2B_2$) +51.06 | $C_s$ ($^2A'$) +135.09 | $C_s$ ($^2A'$) +142.07 | $C_s$ ($^2A'$) +167.12 | $C_s$ ($^2A'$) +168.18

***Fig S3.*** Optimized geometries of top ten low-lying isomers of $LiB_2O_3^-$ along with their relative energies in kcal/mol at MPW1PW91. Also shown are the relative energies at the {CCSD(T)//MPW1PW91} level for top five low-lying isomers.

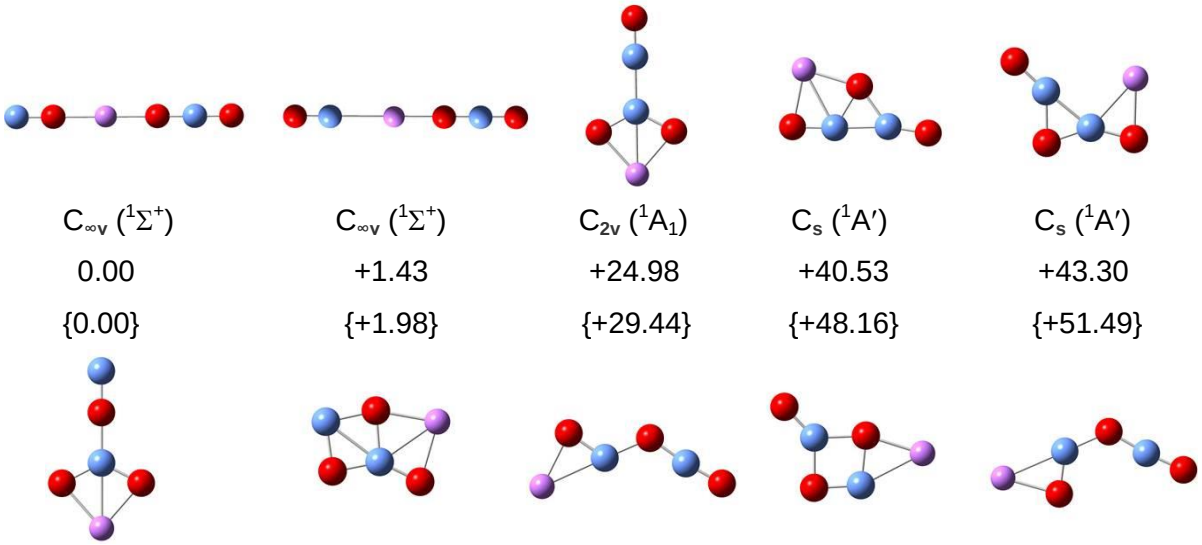

| $C_{\infty v}$ ($^1\Sigma^+$) | $C_{\infty v}$ ($^1\Sigma^+$) | $C_{2v}$ ($^1A_1$) | $C_s$ ($^1A'$) | $C_s$ ($^1A'$) |
|---|---|---|---|---|
| 0.00 | +1.43 | +24.98 | +40.53 | +43.30 |
| {0.00} | {+1.98} | {+29.44} | {+48.16} | {+51.49} |

| $C_{2v}$ ($^1A_1$) | $C_s$ ($^1A'$) | $C_s$ ($^1A'$) | $C_s$ ($^1A'$) | $C_s$ ($^1A'$) |
|---|---|---|---|---|
| +44.08 | +49.68 | +51.81 | +52.12 | +53.30 |

***Fig S4.*** Optimized geometries of top ten low-lying isomers of $AuB_2O_3^-$ along with their relative energies in kcal/mol at MPW1PW91. Also shown are the relative energies at the {CCSD(T)//MPW1PW91} level for top five low-lying isomers.

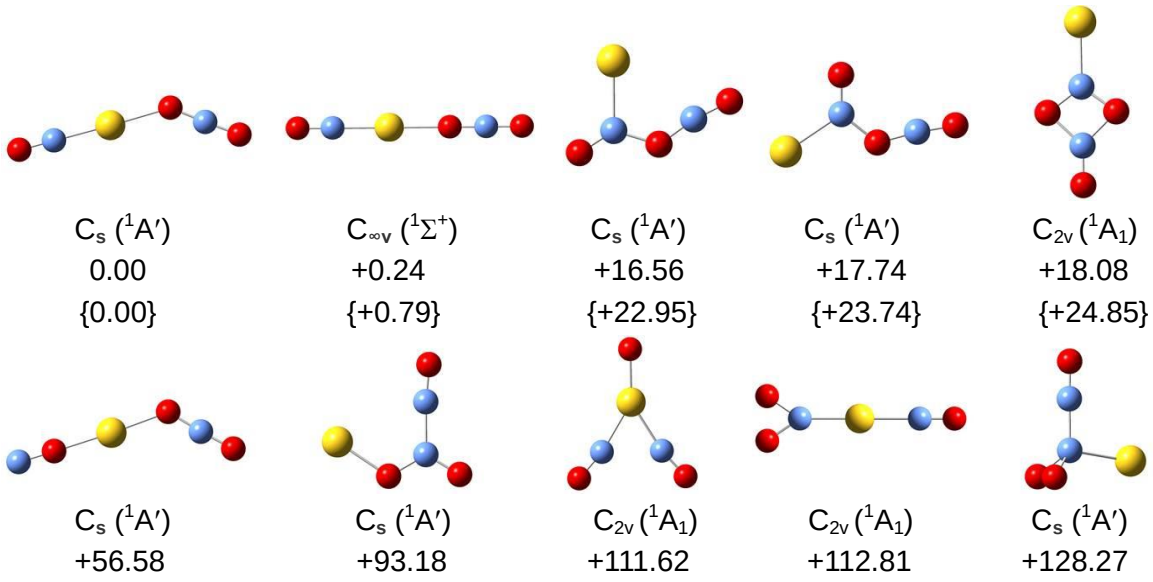

***Fig S5.*** Optimized geometries of top ten low-lying isomers of $LiAuB_2O_3^-$ along with their relative energies in kcal/mol at MPW1PW91. Also shown are the relative energies at the {CCSD(T)//MPW1PW91} level for top five low-lying isomers.

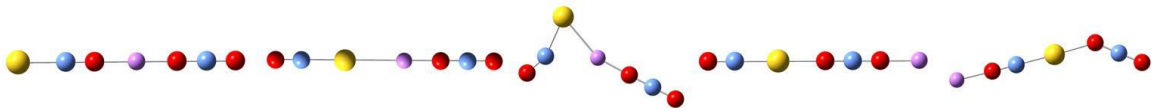

$C_{\infty v}$ ($^2\Sigma^+$) 0.00 {0.00}



$C_{\infty v}$ ($^2\Sigma^+$) +8.43 {+8.69}



$C_s$ ($^2A'$) +12.92 {+11.37}



$C_s$ ($^2A'$) +14.94 {+12.79}



$C_s$ ($^2A'$) +20.35 {+17.36}

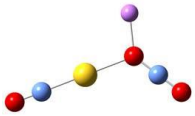

$C_s$ ($^2A'$) +23.29

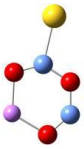

$C_s$ ($^2A'$) +28.24

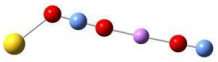

$C_s$ ($^2A'$) +37.64

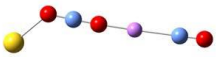

$C_s$ ($^2A'$) +38.91

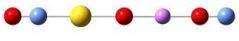

$C_{\infty v}$ ($^2\Sigma^+$) +84.94

***Fig S6.*** Pictures of molecular orbitals for $C_{2v}$ $B_2O_3^-$.

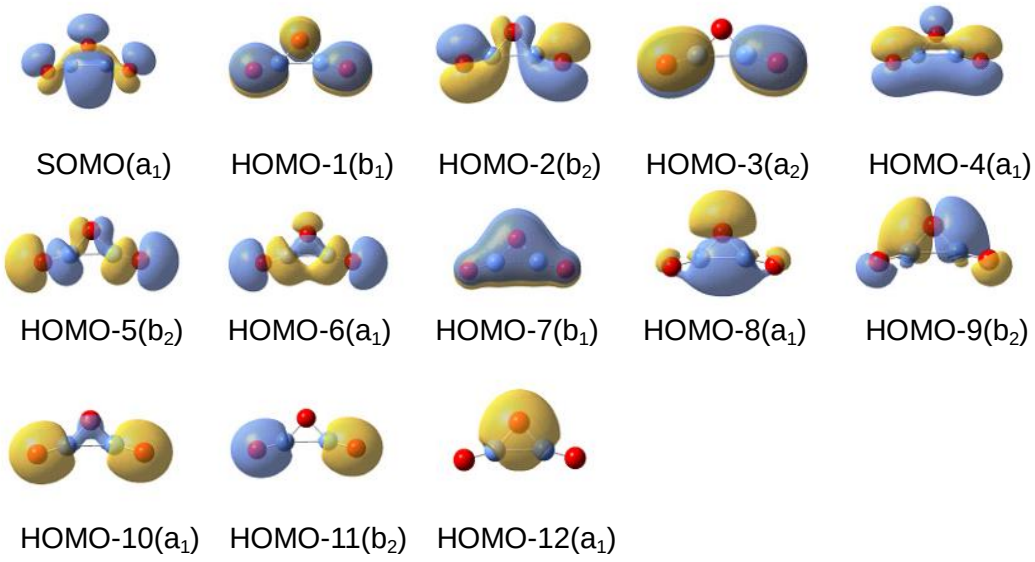


**MO analysis:**

HOMO-10 to HOMO-12 are O 2s lone-pairs. HOMO-1/HOMO-3, HOMO-2/HOMO-4, and HOMO-5/HOMO-6 combine for two B≡O triple bonds. HOMO-8/HOMO-9 represent the apex O–B single bonds. HOMO-7 is primarily an O 2p lone-pair. The SOMO is mainly a 2c-1e BB bond.

***Fig S7.*** Pictures of molecular orbitals for $C_{\infty v}$ $LiB_2O_3^-$.

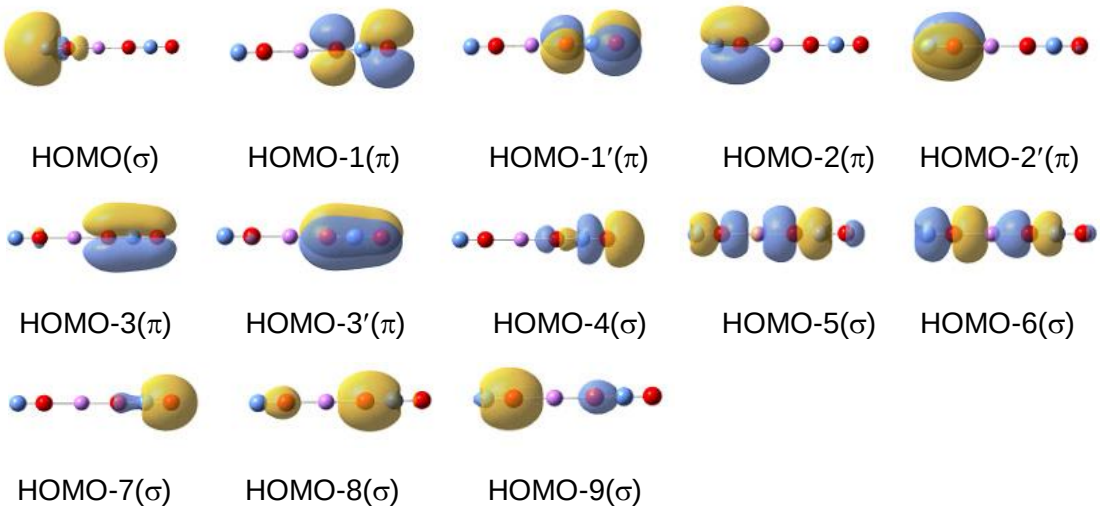


**MO analysis:**

HOMO-7 to HOMO-9 are O 2s lone-pairs. HOMO-2/HOMO-2′/HOMO-6 are the boronyl triple bond. HOMO-4/HOMO-5 are roughly the two B–O σ bonds within the OBO subunit. HOMO-3/ HOMO-1 form a 3c-4e π bond, and HOMO-3′/HOMO-1′ form a second 3c-4e π bond, where HOMO-1 and HOMO-1′ are essentially nonbonding in nature. HOMO is primarily a B 2s lone-pair.

***Fig S8.*** Pictures of molecular orbitals for $C_s$ $AuB_2O_3^-$.

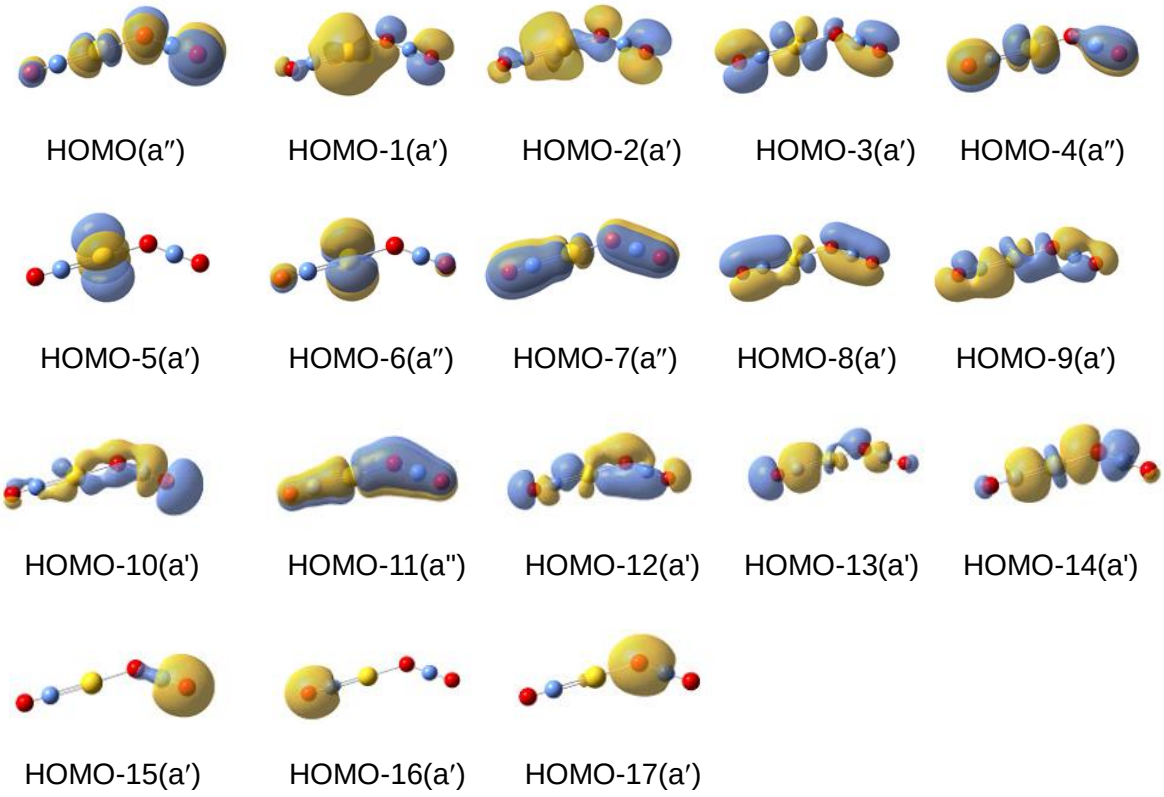


**MO analysis:**

The MOs are highly mixed. Rough analyses are as follows: HOMO-15 to HOMO-17 are O 2s lone-pairs. HOMO-1, HOMO-3, HOMO-4, HOMO-5, and HOMO-6 show Au 6s/5d lone-pair characters. HOMO-10/HOMO-13/HOMO-14 are three BO σ bonds. HOMO-2/HOMO-8/ HOMO-12 are responsible for the OBO π bonds in the $p_y$ manifold, where HOMO-2/ HOMO-12 are primarily a 3c-4e bond in the OBO subunit, with HOMO-2 being essentially nonbonding. Similarly, HOMO/HOMO-7/HOMO-11 are responsible for the OBO π bonds in the $p_z$ manifold, also featuring a 3c-4e hyperbond. HOMO-9 represents the B-Au σ single bond.

***Fig S9.*** Pictures of molecular orbitals for $C_{\infty v}$ $LiAuB_2O_3^-$.

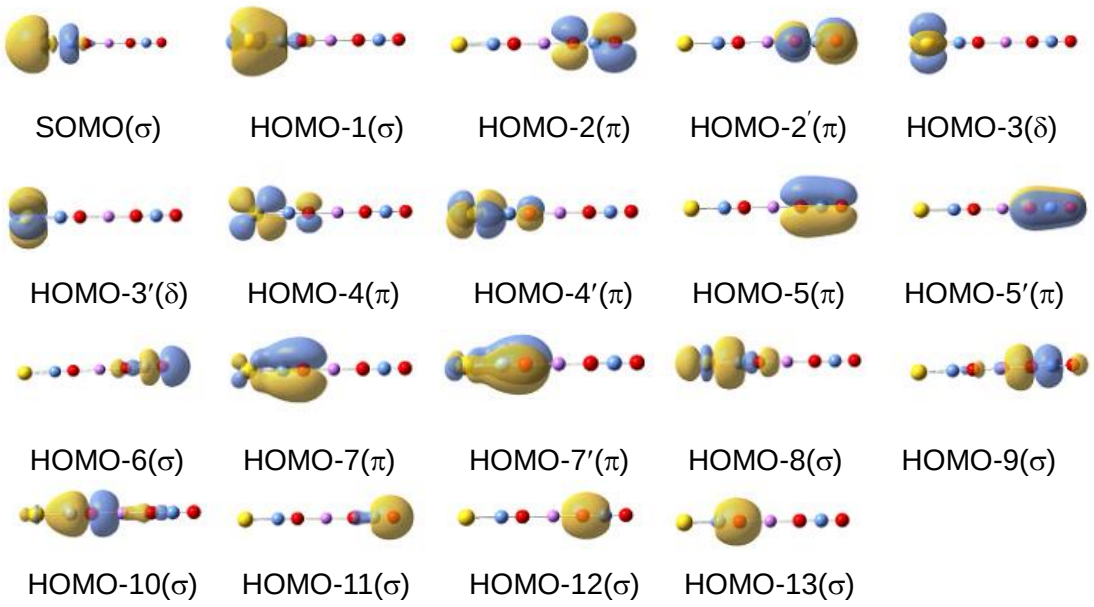


**MO analysis:**

HOMO-11 to HOMO-13 are O 2s lone-pairs. HOMO-3/HOMO-3′/HOMO-4/HOMO-4′/ HOMO-1 are primarily Au lone-pairs. HOMO-7/HOMO-7′/HOMO-10 define the boronyl triple bonds. HOMO-6/HOMO-9 are two σ bonds in the OBO subunit. HOMO-2′/HOMO-5′ form a 3c-4e OBO π bond in the $p_y$ manifold, where HOMO-2′ is essentially nonbonding. Similarly, HOMO-2/HOMO-5 are responsible for a 3c-4e OBO π bond in the $p_z$ manifold. HOMO-8 is the Au-B σ single bond, whereas SOMO is primarily Au 6s in character.

***Figure S10.*** Natural charge distribution of optimized ground-state structures of $B_2O_3^-$, $LiB_2O_3^-$, $AuB_2O_3^-$ and $LiAuB_2O_3^-$ (a–d) and their neutral structures (e-h).